Greek Letters

β = upward propagation rate of Kynch characteristics, or locus of constant concentration in a concentration gradient
θ = thickener flux, volume of solids per unit time per unit area moving down thickener
ρ_f = density of fluid
ρ_s = density of solids
ψ = solids pressure

LITERATURE CITED

Dixon, D. C., "Momentum-Balance Aspects of Free-Settling Theory," *Separation Sci.*, **12**(2), 171, 193 (1977).
Fitch, B., "Biological Treatment of Sewage and Industrial Wastes," **2**, 159, Reinhold, New York (1958).
Fitch, B., "Sedimentation Process Fundamentals," *Trans. Amer. Inst. Mining Eng.*, **223**, 129 (1962).
Fitch, B., "Current Theory and Thickener Design," *Ind. & Eng. Chem.*, **58**, 18 (1966).
Fitch, B., "Current Theory and Thickener Design, 1975," *Filtration and Separation*, **12**, 355, 480, 636 (1975).
Fitch, B., "Sedimentation of Flocculent Suspensions, State of the Art," *AIChE J.*, **25**, 913 (1979).
Gaudin, A. M., and M. C. Fuerstenau, "The Transviewer-X Rays to Measure Suspended Solids Concentration," *Eng. Min. J.*, **159**, 110 (Sept. 1958).
Kynch, G. J., "A Theory of Sedimentation," *Trans. Faraday Soc.*, **48**, 166 (1952).
Michaels, A. S., and J. C. Bolger, "Settling Rates and Sediment Volumes of Flocculated Kaolin Suspensions," *I. & E.C. Fund.*, **1**, 24 (1962).
Shannon, P. T., E. Stroupe, and E. M. Tory, "Batch and Continuous Thickening," *I. and E.C. Fund.*, **2**, 203 (1936).
Shirato, M., Kato, K. Kobayashi, and H. Sakazaki, "Analysis of Settling of Thick Slurries Due to Consolidation," *J. Chem. Eng. Japan*, **3**, 98 (1970).
Talmage, W. P., and E. B. Fitch, "Determining Thickener Unit Areas," *I. & E.C.*, **47**, 38 (1955).
Tiller, F. M., "Revision of Kynch Sedimentation Theory," *AIChE J.*, **27**, 823 (1981).
Tory, E. M., "Batch and Continuous Thickening of Slurries," PhD Thesis, Purdue University (1961).
Yoshioka, N., Y. Hotta, S. Tanaka, S. Naito, and S. Tsugami, "Continuous Thickening of Homogeneous Flocculated Slurries," *Kagaku Kogaku*, **21**, 66 (1957).

Manuscript received June 5, 1981; revision received July 6, and accepted August 26, 1982.

Forced Convection in Three-Dimensional Flows:

III. Asymptotic Solutions with Viscous Heating

W. E. STEWART and M. A. McCLELLAND

Department of Chemical Engineering
University of Wisconsin
Madison, WI 53706

Matched asymptotic solutions are given for the temperature profiles and heat transfer rates in laminar three-dimensional flows with viscous dissipation. The results are asymptotically valid for small thermal diffusivity α; they hold for Newtonian or non-Newtonian fluids. The fluid properties are evaluated at an average temperature for the system; this is satisfactory for moderate temperature differences. Heat transfer formulas for various thermal boundary conditions are included. Several examples are analyzed, including the frictional heating of a polymer melt in flow through a wire-coating die.

SCOPE

Small-diffusivity asymptotes give useful understanding of heat and mass transfer operations. Parts I and II of this series (Stewart, 1963; Stewart, Angelo and Lightfoot, 1970) dealt with boundary-layer phenomena in the absence of viscous heating. The present paper adds the effects of viscous heating in the boundary layers and in the bulk of the fluid. The results are relevant to wire-coating, extrusion, and other flow processes involving heat transport with rapid deformation or highly viscous fluids.

This treatment holds for laminar nonseparated regions of external flows, and for laminar nonseparated thermal entrance regions of internal flows. The velocity profiles are considered as given or separately calculable. The physical properties are treated as constants, evaluated at an average temperature for the given problem.

The superposition principle is used extensively in this paper. The temperature profiles are derived as sums of dissipation and heat-transfer contributions. The dissipation rate itself can be expressed as a sum of simpler functions. By a special choice of such functions, we obtain new similarity solutions which are superimposed to solve Eq. 18.

Parts I and II of the series have been published in *AIChE J.* in 1963 and 1970, respectively. See the Literature Cited section for complete information.

CONCLUSIONS AND SIGNIFICANCE

Frictional heating can significantly alter heat transfer rates to viscous fluids (Eqs. 50 and 51), and can cause overheating in wire-drawing and extrusion processes (Figure 9). The present asymptotic solutions allow quick assessment of these effects and offer insights not readily gained from numerical simulations.

The basic results of this analysis are the inner and outer solutions given in Eqs. 46, 15 and 55. These may be combined with the superposition formulas of Papers I and II (Stewart, 1963; Stewart, Angelo and Lightfoot, 1970) to predict the temperature profiles and heat transfer rates in three-dimensional flows once the velocity profiles are given. The resulting general formulas for steady-state systems are given in Eqs. 48–52. Various applications of the theory are given in Eqs. 56 to 94.

For fluids with small thermal diffusivities, α, the enthalpy increase caused by viscous heating is of order $\alpha^{-1/3}$ in boundary layers that are steady as viewed from the nearest interfacial element. The increase is of order α^0 in time-dependent boundary layers and is of order α^0 outside the boundary layers both for steady and unsteady flows. The order $\alpha^{-1/3}$ agrees with that found by Meksyn (1960) for the steady laminar boundary layer on a flat plate at high Prandtl numbers. A somewhat stronger dependence, $\alpha^{-1/2}$, holds for steady laminar boundary layers at Prandtl numbers near unity (Pohlhausen, 1921).

INTRODUCTION

For complex flows with viscous dissipation, it is difficult and time-consuming to solve the equations of change in full detail. However, useful asymptotes are obtainable for heat transfer by considering the limiting case of small thermal diffusivity.

Paper I of this series (Stewart, 1963) gave asymptotic solutions for forced convection near fixed interfaces, with viscous dissipation neglected. The boundary layers considered there were at steady state when viewed from any interfacial element.

Paper II (Stewart et al., 1970) dealt with forced convection near mobile interfaces. The boundary layers considered there were time-dependent as viewed from the nearest interfacial element. The analysis included internal heat sources, but viscous dissipation was not explicitly treated.

In this work the results of Papers I and II are extended to include viscous dissipation. We use the continuity and energy equations for a constant-property fluid

$$(\nabla \cdot V) = 0 \tag{1}$$

$$\frac{DT}{Dt} - \alpha \nabla^2 T = -\frac{(\tau : \nabla V)}{\rho \hat{C}_p} \tag{2}$$

and treat the velocity field as given.

Particular integrals of Eq. 2 are derived here as matched asymptotic solutions for the boundary layers and the main flow region. The complementary solutions from Papers I and II can be superimposed on these results to describe the combined effects of interfacial heat transfer and viscous dissipation. The combined solutions are given explicitly for steady-state systems in Eqs. 48–52.

COORDINATES AND VELOCITIES

The steady-state inner (boundary layer) solution is done in the curvilinear coordinates x, y and z of Paper I. The coordinate x is measured along the surface streamlines; simplifications for two-dimensional systems will be considered later. The coordinate y is the normal distance from the surface, and the surface coordinate z is measured normal to the local x-direction. In the neighborhood of a given interface these coordinates are orthogonal, with scale factors defined by

$$dr = \delta_x h_x dx + \delta_y h_y dy + \delta_z h_z dz. \tag{3}$$

The scale factor h_y is unity here, and h_x and h_z are taken at their interfacial values.

The steady-state outer (main flow) solution is done in streamline coordinates, Figure 1. Each streamline is given by the intersection of two stream sheets of constant ψ_1 and ψ_2, and each point on a streamline is identified by l, the arc length measured downstream from a reference surface.

The velocity components for the steady-state inner solution are taken from Paper I. They reduce to

$$V_x^{(i)} = y\beta(x,z) + O(y^2) \tag{4}$$

$$V_y^{(i)} = -\frac{y^2}{2h_x h_z}\frac{\partial}{\partial x}(h_z\beta) + O(y^3) \tag{5}$$

$$V_z^{(i)} = 0 + O(y^2) \tag{6}$$

in the absence of net mass transfer. These expressions satisfy Eq. 1 to first order in y. The nonnegative function β is the interfacial magnitude of the rate-of-strain tensor as defined by Bird, Armstrong and Hassager (1977). A particular flow field is described (to the indicated orders in y) by specifying the surface coordinate grid and the rate-of-strain function $\beta(x,z)$.

For the subsequent matching of inner and outer solutions, we need to express Eq. 4 in the coordinates of Figure 1. The continuity equation is automatically satisfied by setting

$$V = [\nabla\psi_1 \times \nabla\psi_2] \tag{7}$$

which may be applied in the boundary layer coordinates (x,y,z) to give

$$V^{(i)} = \begin{vmatrix} \delta_x & \delta_y & \delta_z \\ \frac{1}{h_x}\frac{\partial\psi_1}{\partial x} & \frac{1}{h_y}\frac{\partial\psi_1}{\partial y} & \frac{1}{h_z}\frac{\partial\psi_1}{\partial z} \\ \frac{1}{h_x}\frac{\partial\psi_2}{\partial x} & \frac{1}{h_y}\frac{\partial\psi_2}{\partial y} & \frac{1}{h_z}\frac{\partial\psi_2}{\partial z} \end{vmatrix} \tag{8}$$

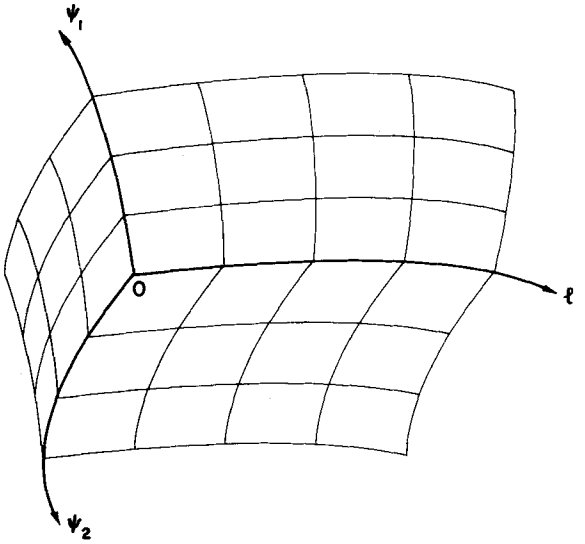

Figure 1. Coordinates (l,ψ_1,ψ_2) for outer solution.

This expression agrees with Eqs. 4–6 to the orders indicated there, if we take the stream functions in the forms

$$\psi_1 = \frac{y^2}{2} h_z\beta + O(y^3) \tag{9}$$

$$\psi_2 = z + C + O(y) \tag{10}$$

with C an arbitrary constant. Hence, Eq. 4 can be rewritten as

$$V_x^{(i)} = \sqrt{2\psi_1\beta/h_z} + O(\psi_1) \tag{11}$$

in the coordinates of Figure 1.

OUTER SOLUTION FOR STEADY FLOWS

At a distance from the boundaries, the heat conduction term of Eq. 2 can be neglected as $\alpha \to 0$. For steady-state conditions this equation then becomes

$$\rho\hat{C}_p(\boldsymbol{V}\cdot\nabla T^{(o)}) = -(\boldsymbol{\tau}:\nabla\boldsymbol{V}) \tag{12}$$

which may be rewritten in the streamline coordinates as

$$\rho\hat{C}_p V\frac{\partial T^{(o)}}{\partial l} = -(\boldsymbol{\tau}:\nabla\boldsymbol{V}). \tag{13}$$

Integration of this equation with the initial condition

$$T = T_\infty \text{ at } l = 0 \tag{14}$$

yields the outer temperature profile

$$T^{(o)}(l,\psi_1,\psi_2) - T_\infty = \frac{1}{\rho\hat{C}_p}\int_0^l \frac{-(\boldsymbol{\tau}:\nabla\boldsymbol{V})}{V} dl_1 \tag{15}$$

which is well behaved, except near stationary boundaries where V vanishes and $(\boldsymbol{\tau}:\nabla\boldsymbol{V})$ does not. Near such boundaries, heat conduction becomes important and an inner solution is required.

The subsequent matching of solutions will require the asymptote of Eq. 15 for the boundary region. To order $\sqrt{\psi_1}$ we may set $V = V_x^{(i)}$, $dl = h_x dx$, and

$$-(\boldsymbol{\tau}:\nabla\boldsymbol{V}) = \tau_0(x,z)\beta(x,z) + O(\sqrt{\psi_1}) \tag{16}$$

in which $\tau_0(x,z)$ is the wall shear stress. The resulting asymptote of Eq. 15 near stationary boundaries is

$$\lim_{\psi_1\to 0}\sqrt{2\psi_1}\,[T^{(o)}(l,\psi_1,\psi_2) - T_\infty] = \frac{1}{\rho\hat{C}_p}\int_0^x \tau_0\sqrt{h_z\beta}\,h_x dx_1 \tag{17}$$

with $l = \int_0^x h_x dx_1$ in this limit.

INNER SOLUTION FOR STEADY FLOWS

Equation 2 can be simplified according to the usual boundary layer approximations (Schlichting, 1960; Rosenhead, 1963). In the limit of small α, the Laplacian $\nabla^2 T$ in the boundary layers reduces essentially to the second normal derivative, $\partial^2 T/\partial y^2$. In the same limit, Eq. 16 describes the viscous dissipation in the boundary layers. With these substitutions, and use of Eqs. 4, 5 and 6, the energy equation becomes

$$\frac{y\beta}{h_x}\frac{\partial T^{(i)}}{\partial x} - \frac{y^2}{2h_xh_z}\frac{\partial}{\partial x}(h_z\beta)\times\frac{\partial T^{(i)}}{\partial y} = \alpha\frac{\partial^2 T^{(i)}}{\partial y^2} + \frac{\tau_0\beta}{\rho\hat{C}_p} \tag{18}$$

for steady-state boundary layers in the limit of small α. Since no z-derivatives remain, Eq. 18 can be integrated in two dimensions with z as a parameter.

Equation 18 can be solved conveniently by representing $\tau_0\beta$ as a superposition of special functions $\epsilon(x,\xi,z)$, each chosen to allow a similarity solution. Each ϵ-function has a different value of the location parameter ξ, and vanishes for $x < \xi$. A corresponding family of solutions $T^{*(i)}$ is defined by the differential equation

$$\frac{y\beta}{h_x}\frac{\partial T^{*(i)}}{\partial x} - \frac{y^2}{2h_xh_z}\frac{\partial}{\partial x}(h_z\beta)\times\frac{\partial T^{*(i)}}{\partial y} = \alpha\frac{\partial^2 T^{*(i)}}{\partial y^2} + \frac{\epsilon(x,\xi,z)}{\rho\hat{C}_p}, \tag{19}$$

and the boundary conditions

$$\frac{\partial T^{*(i)}}{\partial y} = 0 \text{ at } y = 0 \tag{20}$$

$$T^{*(i)} \to T_\infty \text{ as } y \to \infty \tag{21}$$

$$T^{*(i)} = T_\infty \text{ for } x < \xi. \tag{22}$$

Once the functions $\epsilon(x,\xi,z)$ are found, these and the resulting solutions $T^{*(i)}$ can be superimposed to solve Eq. 18 for an adiabatic boundary.

We postulate a similarity solution for $T^{*(i)}$,

$$T^{*(i)} - T_\infty = f(x,\xi,z)g(\eta) \tag{23}$$

with

$$\eta = \frac{y}{\delta(x,\xi,z)}. \tag{24}$$

This postulate parallels that used by Stewart (1963) to solve Eq. 18 without the dissipation term. Here $\delta(x,\xi,z)$ is a boundary layer thickness, which (in view of Eq. 22) is taken to vanish for $x < \xi$. The boundary conditions 20 and 21 then reduce to

$$\frac{dg}{d\eta} = 0 \text{ at } \eta = 0 \tag{25}$$

$$g \to 0 \text{ as } \eta \to \infty. \tag{26}$$

Insertion of the postulates (Eqs. 23 and 24) into Eq. 19 gives

$$\left[\frac{\delta^3\beta}{\alpha h_x f}\frac{\partial f}{\partial x}\right]\eta g - \left[\frac{\delta^2\beta}{\alpha h_x}\frac{\partial\delta}{\partial x} + \frac{\delta^3}{2\alpha h_x h_z}\times\frac{\partial}{\partial x}(h_z\beta)\right]\eta^2\frac{dg}{d\eta} = \frac{d^2g}{d\eta^2} + \left[\frac{\delta^2\epsilon}{kf}\right]. \tag{27}$$

The postulates hold only if the bracketed terms are independent of x, for $x \geq \xi$:

$$\frac{\delta^2\beta}{\alpha h_x}\frac{\partial\delta}{\partial x} + \frac{\delta^3}{2\alpha h_x h_z}\frac{\partial}{\partial x}(h_z\beta) \equiv \frac{\delta^2\sqrt{h_z\beta}}{\alpha h_x h_z}\frac{\partial}{\partial x}(\delta\sqrt{h_z\beta}) = C_0(z) \tag{28}$$

$$\frac{\delta^3\beta}{\alpha h_x}\frac{\partial lnf}{\partial x} = C_1(z) \tag{29}$$

$$\frac{\delta^2\epsilon}{kf} = C_2(z). \tag{30}$$

The functions $C_i(z)$ may be taken as positive constants. Choosing $C_0 = 3$ and integrating Eq. 28 with the initial condition

$$\sqrt{h_z\beta}\,\delta(x,\xi,z) = 0 \text{ at } x = \xi \tag{31}$$

required by Eq. 22, we obtain the boundary layer thickness

$$\delta = \frac{1}{\sqrt{h_z\beta}}\left\{9\alpha\int_\xi^x \sqrt{h_z\beta}\,h_x h_z\,dx_1\right\}^{1/3} \qquad (x \geq \xi). \tag{32}$$

The choice $C_2 = 1$ gives an expression for ϵ:

$$\epsilon = kf/\delta^2 \tag{33}$$

Equations 28 and 29 give the following differential equation for f,

$$\frac{\partial lnf}{\partial x} = \frac{C_1}{C_0}\frac{\partial ln(\delta\sqrt{h_z\beta})}{\partial x} \qquad (x \geq \xi) \tag{34}$$

which may be integrated to give

$$f = C_3(z)(\delta\sqrt{h_z\beta})^r \qquad (x \geq \xi). \tag{35}$$

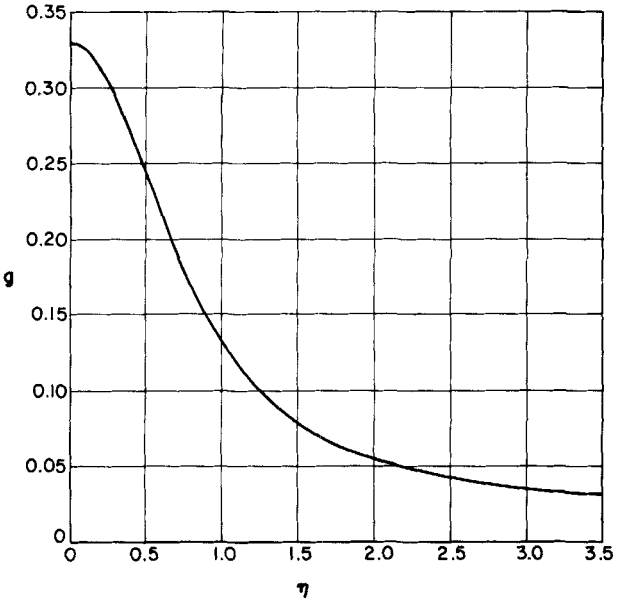

Figure 2. Boundary layer temperature function $g(\eta)$; solution of Eqs. 25, 26 and 41.

Here $C_3(z)$ is a function of integration, and $r = C_1/C_0$.

The constant r is determined by matching the inner and outer solutions. The outer limit of the inner solution for $x \geq \xi$ has the form

$$\lim_{y\to\infty} \{y[T^{*(i)} - T_\infty]\} = \frac{f\delta}{C_0(1+r)} \tag{36}$$

according to Eqs. 23–24 and 26–30. Insertion of Eq. 35 and $C_0 = 3$ gives the limit as

$$\lim_{y\to\infty} \{y[T^{*(i)} - T_\infty]\} = \frac{C_3(z)\delta^{r+1}(h_z\beta)^{r/2}}{3(1+r)}. \tag{37}$$

The inner limit, Eq. 17, of the outer solution may be rewritten for the source distribution $\epsilon(x,\xi,z)$ to give

$$\lim_{\psi_1\to 0} \{\sqrt{2\psi_1}\,[T^{*(o)} - T_\infty]\} = \frac{1}{\rho\hat{C}_p}\int_\xi^x \epsilon\sqrt{h_z/\beta}\,h_x dx_1. \tag{38}$$

Here ξ has replaced zero as the lower limit of integration. Insertion of Eqs. 33 and 35 for ϵ, and Eq. 9 for ψ_1, gives the limit as

$$\lim_{y\to 0} \{y[T^{*(o)} - T_\infty]\} = \frac{\alpha C_3(z)}{\sqrt{h_z\beta}}\int_\xi^x h_x h_z \delta^{r-2}(h_z\beta)^{(r-1)/2}\,dx_1. \tag{39}$$

The limits in Eqs. 37 and 39 match if and only if $r = 2$. With this choice, we obtain

$$\lim_{y\to\infty} \{y[T^{*(i)} - T_\infty]\} = \lim_{y\to 0} \{y[T^{*(o)} - T_\infty]\} = \frac{C_3(z)\delta^3 h_z\beta}{9}. \tag{40}$$

Equation 27 then becomes

$$6\eta g - 3\eta^2\frac{dg}{d\eta} = \frac{d^2g}{d\eta^2} + 1 \tag{41}$$

which may be solved numerically with Eqs. 25 and 26 as boundary conditions. The resulting interfacial value of the function g is

$$g(0) = 0.32973 \tag{42}$$

and the function $g(\eta)$ is shown in Figure 2. The outer limit given in Eq. 40 corresponds to the asymptotic expression $(9\eta)^{-1}$ for the function $g(\eta)$.

The function $C_3(z)$ in Eq. 35 remains to be determined. Equations 33 and 35 give, for $r = 2$,

$$C_3(z) = \frac{\epsilon}{kh_z\beta} \quad (x \geq \xi). \tag{43}$$

By definition, ϵ vanishes for $x < \xi$; thus, $\epsilon/h_z\beta$ is a step function of x on any given surface streamline. Insertion of Eqs. 43, 32 and 35 with $r = 2$ into Eq. 23 then gives

$$T^{*(i)} - T_\infty = \frac{9^{2/3}}{\rho\hat{C}_p\alpha^{1/3}}\,g(\eta) \times\left(\int_{x_1=\xi}^x \sqrt{h_z\beta}\,h_x h_z dx_1\right)^{2/3}\left.\frac{\epsilon}{h_z\beta}\right|_{\xi,z} \tag{44}$$

as the fundamental inner solution for $x \geq \xi$. Upstream of this region, Eq. 22 applies.

We now return to the solution of Eq. 18 with an adiabatic boundary at $y = 0$, a uniform upstream temperature T_∞ for $x < 0$, and an arbitrary shear stress distribution $\tau_0(x,z)$ on the wall for $x \geq 0$. The amplitudes of the step functions $\epsilon/h_z\beta$ are now chosen by specifying

$$\frac{\tau_0}{h_z} = \int_{\xi=0_-}^x d\left(\frac{\tau_0}{h_z}\right)\Big|_{\xi,z} = \int_{\xi=0_-}^x d\left(\frac{\epsilon}{h_z\beta}\right)\Big|_{\xi,z} \tag{45}$$

thus equating the steps to increments of τ_0/h_z. Doing likewise in Eq. 44 and superimposing the results, we obtain the inner solution

$$T_A^{(i)} - T_\infty = \frac{9^{2/3}}{\rho C_p\alpha^{1/3}}\int_{\xi=0_-}^x g\left(\frac{y}{\delta(x,\xi,z)}\right) \times\left(\int_{x_1=\xi}^x \sqrt{h_z\beta}\,h_x h_z dx_1\right)^{2/3} d\left(\frac{\tau_0}{h_z}\right)\Big|_{\xi,z}. \tag{46}$$

for the case of an adiabatic boundary. The outer limit of this solution matches the inner limit of Eq. 15. The outer integrations in Eqs. 45 and 46 are begun from $\xi = 0_-$, with τ_0 initially zero to conform to the ϵ-functions. This initial stress value is true for a stagnation locus; it is artificial in most other cases.

For calculation of surface temperatures ($y = 0$), Eq. 46 can be integrated by parts to give

$$T_{A,0}^{(i)} - T_\infty = \frac{9^{2/3}g(0)}{\rho\hat{C}_p\alpha^{1/3}}\int_{\xi=0_+}^x \frac{2}{3} \times\left(\int_{x_1=\xi}^x \sqrt{h_z\beta}h_x h_z dx_1\right)^{-1/3}\tau_0\sqrt{h_z\beta}\,h_x|_{\xi,z}d\xi. \tag{47}$$

This result is convenient for flows past submerged objects with sharp edges or corners, where the representation of $(\tau_0/h_z)|_{\xi,z}$ may be singular as in Eq. 57. The limiting process needed to apply Eq. 46 in such cases is already done for $y = 0$ in Eq. 47.

Results for nonadiabatic boundaries may be obtained by combining the present results with those of Stewart (1963). In that work Eq. 2 was solved without the dissipation term, with a uniform upstream temperature T_∞ and with arbitrary interfacial thermal conditions for $x \geq 0$. Since Eq. 2 is linear, we may superimpose Eq. 25 of the 1963 paper upon the particular solution just found; this yields the following temperature profile for the case of a given surface temperature distribution $T_0(x,z)$:

$$T(x,y,z) = T_A(x,y,z) + \int_{0_-}^x [1 - \Pi(\eta)]|_{\xi,x,y,z}\,d(T_0 - T_{0,A})|_{\xi,z}. \tag{48}$$

Here $T_{0,A}$ is obtained from Eq. 47, or from Eq. 46 with $y = 0$; also

$$\Pi(\eta) = \frac{1}{\Gamma(4/3)}\int_0^\eta \exp(-\eta_1^3)d\eta_1 \tag{49}$$

with η defined by Eqs. 24 and 32. The resulting interfacial heat flux is

$$q_0 = -k\left.\frac{\partial T}{\partial y}\right|_{y=0}$$

$$= \frac{k\sqrt{h_z\beta}}{(9\alpha)^{1/3}\Gamma(4/3)}\int_{\xi=0_-}^x \left\{\int_{x_1=\xi}^x \sqrt{h_z\beta}\,h_x h_z dx_1\right\}^{-1/3} d(T_0 - T_{0,A})|_{\xi,z} \tag{50}$$

and the total heat transfer rate through a surface region $0 \le x < x_2(z)$, $z_I < z < z_{II}$ is

$$Q = \frac{3^{1/3}k}{2\Gamma(4/3)\alpha^{1/3}} \int_{z_I}^{z_{II}} \int_{\xi=0-}^{x_2(z)} \times \left\{ \int_{x_1=\xi}^{x_2(z)} \sqrt{h_z \beta}\, h_x h_z dx_1 \right\}^{2/3} d(T_0 - T_{0,A})|_{\xi,z}\, dz. \quad (51)$$

A two-dimensional version of Eq. 50 was given by Lighthill (1950), but with an approximate function $T_{0,A}$ based on the calculations of Pohlhausen (1921) for Prandtl numbers near unity. The present results are preferable for large Prandtl numbers.

The temperature profile corresponding to any given surface heat flux distribution $q_0(x,z)$ is obtained by combining Eq. 46 above with Eq. 39 of Stewart (1963):

$$T(x,y,z) = T_A(x,y,z) + \frac{1}{\frac{1}{3}\Gamma\left(\frac{2}{3}\right)\rho\hat{C}_p(9\alpha)^{2/3}} \int_{0-}^{x} \frac{\exp(-\eta^3) q_0 h_x h_z\, d\xi}{\left[\int_{\xi}^{x} \sqrt{h_z \beta}\, h_x h_z dx_1\right]^{2/3}}. \quad (52)$$

This completes the steady-state solutions to lowest order in α.

TRANSIENT SOLUTIONS

For transient processes, an outer solution for $\alpha \to 0$ is obtained by starting from Eq. 2 without the conduction term:

$$\rho\hat{C}_p \frac{DT^{(o)}}{Dt} = -(\tau : \nabla V). \quad (53)$$

The initial condition is taken to be

$$T(X_1,X_2,X_3,t) = T_\infty \text{ at } t = 0. \quad (54)$$

Here the X_i are material coordinates. Integration along the particle paths gives the time-dependent outer solution

$$T^{(o)}(X_1,X_2,X_3,t) - T_\infty = \frac{1}{\rho\hat{C}_p} \int_0^t - (\tau : \nabla V)|_{X_1,X_2,X_3,t_1}\, dt_1 \quad (55)$$

which reduces to Eq. 15 for steady flows.

The transient inner solution for the dissipative temperature rise is obtainable from Eq. 80 of Paper II. In the limit of small α, the dissipation term of Eq. 2 may be approximated in the boundary layer by the local interfacial value. The resulting inner solution for T is independent of the normal coordinate y, and is consequently unaffected by heat conduction. Equation 55 matches this adiabatic inner solution exactly at the interface, and is preferable everywhere else. Thus, for adiabatic time-dependent systems, Eq. 55 is uniformly valid throughout the fluid for small α. This particular integral [with $T^{(o)}$ labelled as T_A] can be superimposed with Eqs. 76–79 of Paper II to describe unsteady-state heat transfer with viscous dissipation. An application of Eq. 55 is given in the final example.

APPLICATIONS TO SIMPLE GEOMETRIES

The flows considered in this section are Newtonian and have uniform temperature upstream from a locus $x = 0$ where significant dissipation begins. Inner solutions are presented for adiabatic boundaries; these may be combined with Eqs. 48–52 to obtain results for other interfacial boundary conditions.

Developed Flows in Ducts

For slow flows of viscous liquids in ducts, the hydrodynamic development region may be considerably shorter than the thermal entrance region. The temperature profiles may then be approximated by assuming abrupt flow development at the entrance of the duct. The x-coordinate for these systems is measured parallel to the flow axis and the z-coordinate is measured around the duct perimeter. The scale factors h_x and h_z are set to unity. Several duct geometries are shown in Figure 3, and the corresponding expressions for β are shown in Table 1. Equation 46 gives the inner solution for the temperature rise,

$$T_A^{(i)} - T_\infty = \frac{(81\nu^2x^2\beta^4\mathrm{Pr})^{1/3}}{\hat{C}_p} g\left(y^3\sqrt{\frac{\beta}{9\alpha x}}\right) \quad (56)$$

and the outer solution is obtainable from Eq. 15.

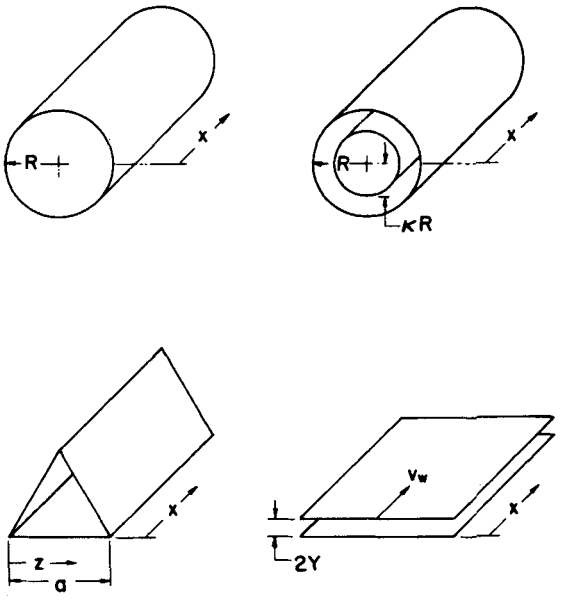

Figure 3. Duct geometries: tube, annulus, equilateral three-walled duct, and slit with one wall moving downstream.

TABLE 1. WALL SHEAR RATES FOR FULLY DEVELOPED NEWTONIAN FLOWS IN DUCTS

Duct Geometry	Wall Shear Rate, β
Tube	$(P_0 - P_L)R/2\mu L$
Annulus: Inner Cylinder	$\frac{(P_0 - P_L)R}{2\mu L}\left[-\kappa + \frac{(1-\kappa^2)}{2\ln(1/\kappa)}\frac{1}{\kappa}\right]$
Outer Cylinder	$\frac{(P_0 - P_L)R}{2\mu L}\left[1 - \frac{(1-\kappa^2)}{2\ln(1/\kappa)}\right]$
Equilateral Three-Walled Duct (Landau and Lifshitz, 1960)	$\frac{\sqrt{3}(P_0 - P_L)}{2\mu L}\frac{z(a-z)}{a}$
Slit with One Wall Moving Downstream:	
Fixed Wall	$\frac{(P_0 - P_L)Y}{\mu L} + \frac{V_w}{2Y}$
Moving Wall	$\left\lvert\frac{(P_0 - P_L)Y}{\mu L} - \frac{V_w}{2Y}\right\rvert$

Wedge Flows

Consider a laminar two-dimensional flow impinging on the wedge shown in Figure 4. The boundary-layer coordinates are rectangular with $h_x = 1$. The velocity profiles are given by Hartree (1937); the interfacial shear rate is

$$\beta = f''(0,m)\left(\frac{m+1}{2}\frac{U^3}{\nu x}\right)^{1/2} \quad (x > 0) \quad (57)$$

Here U is the longitudinal velocity at the outer edge of the boundary layer,

$$U = u_1 x^m \quad (58)$$

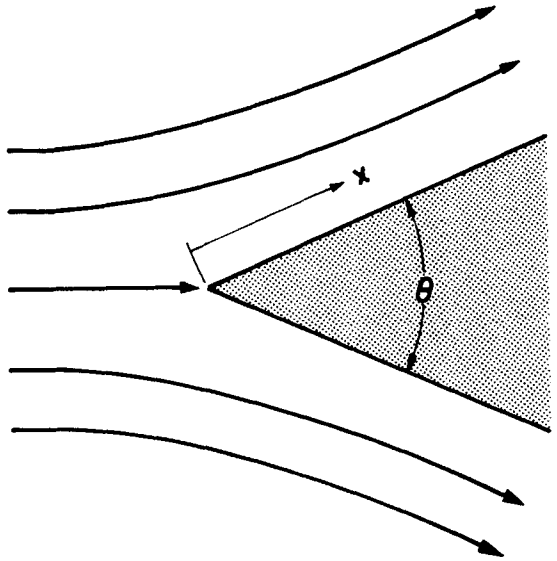

Figure 4. Laminar flow over a wedge.

and the exponent m is given by potential flow theory as

$$m = \theta/(2\pi - \theta). \tag{59}$$

The dimensionless wall stress $f''(0,m)$ is tabulated by Hartree; some values are $f''(0,0) = 0.4696$ for the flat plate and $f''(0,1) = 1.233$ for plane stagnation flow. Equation 46 gives the following surface temperature distribution for flow over an adiabatic wedge, when note is taken of the jump in β (and thus in τ_0/h_z) at $x = 0$:

$$T_{0,A}^{(i)} - T_\infty = \frac{2}{3} 6^{2/3}[f''(0,m)]^{4/3} g(0) B\left(\frac{2}{3}, \frac{9m+1}{3m+3}\right) \frac{U^2 \mathrm{Pr}^{1/3}}{\hat{C}_p}. \tag{60}$$

Equation 47 gives the same result, by a simpler integration. The condition $m > -1/9$, required by Eq. 60, is met for all wedge angles that permit nonseparated flows. For the special case of a flat plate ($m = 0$), the resulting recovery factor is

$$\frac{\hat{C}_p[T_{0,A}^{(i)} - T_\infty]}{\frac{1}{2}U^2} = 1.92\ \mathrm{Pr}^{1/3} \tag{61}$$

in agreement with the large Pr asymptote obtained by Meksyn (1960) for this geometry.

Creeping Flow Around a Sphere

Consider the steady creeping flow of a Newtonian fluid past a stationary sphere. The surface streamlines are contours of constant longitude ϕ, running from $\theta = 0$ to $\theta = \pi$ in spherical coordinates. The surface coordinates for the inner solution are $x = \theta$ and $z = \phi$, with scale factors $h_x = R$ and $h_z = R \sin\theta$. The Stokes velocity profile gives the interfacial shear rate

$$\beta = \frac{3}{2} \frac{V_\infty \sin\theta}{R}. \tag{62}$$

Thus, τ_0/h_z is a step function, vanishing for $x < 0$ and equal to $3\mu V_\infty/2R^2$ for $x \geq 0$. Equation 46 or 47 gives the dissipative temperature rise

$$T_{0,A}^{(i)} - T_\infty = \left(\frac{9}{4}\right)^{4/3} g(0) \frac{\mathrm{Pr}^{1/3}}{\hat{C}_p} \left[\frac{\nu}{R} V_\infty^2 (2\theta - \sin 2\theta)\right]^{2/3} \tag{63}$$

on the surface of an adiabatic sphere.

Slow Flow Around a Cylinder

Consider the slow steady flow of an infinite fluid across a circular cylinder of radius R. The surface streamlines run from $\theta = 0$ to $\theta = \pi$. The surface coordinates for the inner solution are $x = \theta$ and $z = Z$, with scale factors $h_x = R$ and $h_z = 1$, where (r,θ,Z) are the cylindrical coordinates. A series expression for the velocity profile near the cylinder is given by Rosenhead (1963). Using only the leading terms, one obtains the interfacial shear rate

$$\beta = \frac{2V_\infty \sin\theta}{SR}. \tag{64}$$

Here

$$S = \frac{1}{2} - \gamma + \ln(8/Re) \tag{65}$$

and γ is Euler's constant. Equation 46 gives the surface temperature rise due to viscous dissipation as

$$T_{0,A}^{(i)} - T_\infty = \left(\frac{1296\ \nu^2 V_\infty^4 \mathrm{Pr}}{R^2 S^4}\right)^{1/3} \frac{g(0)}{\hat{C}_p} \times \int_{\xi=0-}^{\theta} \left(\int_{\theta_1=\xi}^{\theta} \sqrt{\sin\theta_1}\, d\theta_1\right)^{2/3} \cos\xi\, d\xi. \tag{66}$$

The double integral $I(\theta)$ has been evaluated numerically and is given in Table 2.

TABLE 2. INTEGRAL IN EQ. 66 FOR CYLINDER SURFACE TEMPERATURE

$180\,\theta/\pi$	$I(\theta) = \int_{\xi=0-}^{\theta} \left(\int_{\theta_1=\xi}^{\theta} \sqrt{\sin\theta_1}\, d\theta_1\right)^{2/3} \cos\xi\, d\xi$
0*	0.0000
15	0.0355
30	0.1377
45	0.2951
60	0.4896
75	0.6993
90	0.9008
105	1.073
120	1.198
135	1.267
150	1.278
165	1.243
180	1.195

* Stagnation line.

Flow Near a Rotating Disk

Consider the three-dimensional axisymmetric flow induced by a disk rotating with an angular velocity ω in an otherwise quiescent fluid. A cylindrical coordinate system is chosen which rotates with the disk. From the analysis of Cochran (1934) the surface velocity components are

$$V_r = r\omega F(\zeta) \tag{67}$$

$$V_\theta = r\omega[G(\zeta) - 1] \tag{68}$$

with

$$\zeta = Z\sqrt{\frac{\omega}{\nu}}. \tag{69}$$

From Cochran's tables of the solution, we obtain

$$\beta = \left.\frac{\partial V_t}{\partial Z}\right|_{Z=0} = \left.\frac{\partial}{\partial Z}\sqrt{(V_r^2 + V_\theta^2)}\right|_{Z=0} = r\sqrt{\omega^3/\nu}\,\sqrt{[F'(0)]^2 + [G'(0)]^2} \tag{70}$$

with $F'(0) = 0.510$ and $G'(0) = -0.616$.

Since the temperature is independent of θ, we may choose r and θ as surface coordinates (x,z), whence $h_x = 1$ and $h_z = r$. This is simpler than integration along the spiral surface streamlines, and gives the same result. The inner solution is then done with β replaced by $\beta_r = r\sqrt{\omega^3/\nu}\,F'(0)$ (Eq. 70) except in calculation of the viscous dissipation. In Eqs. 45 and 46, we must accordingly replace

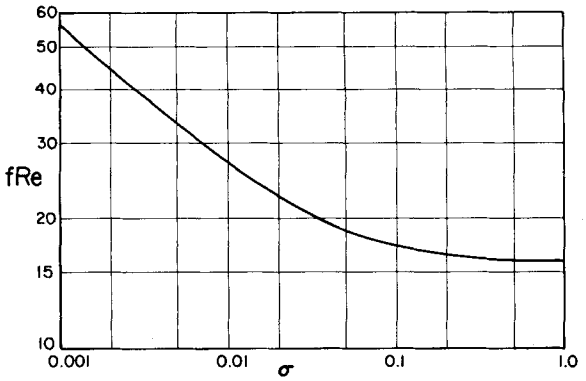

Figure 5. Wall shear stress function for entrance flow in a tube, according to Eq. 73.

$\epsilon/h_z\beta$ by $\epsilon/h_z\beta_r$, and τ_0/h_z by $\tau_0\beta/h_z\beta_r$. The resulting inner solution for the dissipative temperature rise is

$$T_A^{(i)} - T_\infty = \frac{(\omega r)^2 (9\ \mathrm{Pr})^{1/3}}{\hat{C}_p\ [F'(0)]^{2/3}} \{[F'(0)]^2 + [G'(0)]^2\} \times g\left(Z \sqrt[3]{\frac{F'(0)\omega^{3/2}}{3\alpha\nu^{1/2}}}\right) \quad (71)$$

for a thermally insulated disk.

Entrance Flow in a Tube

Consider a fluid which enters a circular tube of radius R with an initially flat velocity profile. From the numerical results of Hornbeck (1964), the quantity

$$f\mathrm{Re} = \frac{-4R}{\langle V\rangle} \left.\frac{\partial V_z}{\partial r}\right|_{r=R} \quad (72)$$

can be computed as a function of downstream distance.

A curve fit of the numerical solutions for fRe is plotted in Figure 5. The fitted expression is

$$f\mathrm{Re} = \frac{1.328\sigma^{-1/2} + 452\sigma^{1.1} + 15.6}{1 + 28.25\sigma^{1.1}} \quad (73)$$

in which

$$\sigma = (x/R)(R\langle V\rangle/\nu)^{-1}. \quad (74)$$

Equation 73 satisfies the asymptotic relations

$$\lim_{\sigma\to 0} f\mathrm{Re} = 1.328\sigma^{-1/2} \quad (75)$$

$$\lim_{\sigma\to\infty} f\mathrm{Re} = 16. \quad (76)$$

Equations 47, 72 and 73 give the surface temperature rise in the entrance region of an adiabatic tube:

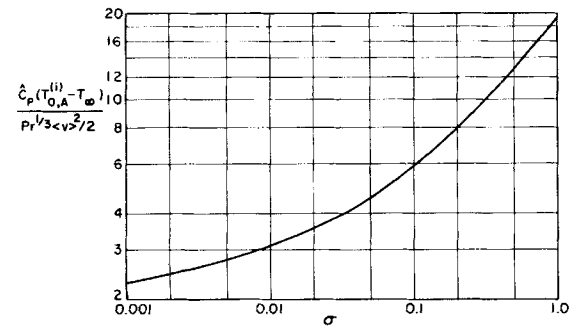

Figure 6. Wall temperature rise for adiabatic entrance flow in a tube.

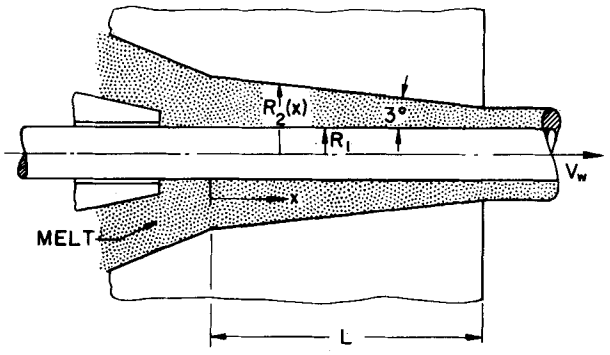

Figure 7. Schematic view of a wire-coating die.

$$T_{0,A}^{(i)} - T_\infty = \frac{\left(\frac{9}{16}\right)^{2/3} g(0)\mathrm{Pr}^{1/3}\langle V\rangle^2}{\hat{C}_p} \times \int_{\xi=0+}^{\sigma} \frac{2}{3}\left(\int_{\sigma_1=\xi}^{\sigma} \sqrt{f\mathrm{Re}}\, d\sigma_1\right)^{-1/3} (f\mathrm{Re}|_\xi)^{3/2} d\xi. \quad (77)$$

This solution is plotted in dimensionless form in Figure 6. Near the entrance, the temperature rise is essentially that of the flat plate, whereas downstream the curve approaches the asymptote of Eq. 56 for hydrodynamically developed laminar flow.

WIRE-COATING PROBLEM

Improvements in wire-coating processes have been made largely by empirical means. Local observations in such flows are difficult, because of the small clearances required in a wire-coating die. Theoretical treatment is hampered by temperature-dependent properties, along with complicated rheology and geometry. Previous theoretical work, summarized by Carley, Endo, and Krantz (1978), has included approximate analytical treatments and elaborate numerical computations. In this section we give an asymptotic analysis of a representative wire-coating operation, to study the viscous heating with a minimum of computation.

The geometry (Figure 7) and operating conditions of a typical wire-coating die are given by Haas and Skewis (1974). Let x be the distance downstream from the inlet of the die. The die wall is tapered, with local radius

$$R_2(x) = a(x)R_1. \quad (78)$$

Here R_1 is the wire radius, and the function $a(x)$ is linear,

$$a(x) = a(0)\left(1 - \frac{x}{L}\right) + a(L)\left(\frac{x}{L}\right) \quad (79)$$

with

$$a(0) = 3.40$$
$$a(L) = 1.79$$
$$L = 0.99\ \mathrm{cm}\ (0.39\ \mathrm{in.})$$
$$R_1 = 0.0323\ \mathrm{cm}\ (0.0127\ \mathrm{in.}).$$

The wire velocity V_w is 20.32 m·s^{-1} (4,000 ft·min^{-1}).

An exact description of the flow field would require numerical integration of the coupled mass, momentum, and energy equations. Here we use an approximate velocity profile, and calculate the viscous heating only in the high-shear region, $x > 0$. The axial velocity profile in the melt is approximated by a three-term expansion

$$\frac{V_x}{V_w} = f_0(x) + f_1(x)ln\left(\frac{r}{R_1}\right) + f_2(x)\left(\frac{r}{R_1}\right)^2 \quad (80)$$

based on functions appropriate to annular Newtonian flow with a moving inner cylinder. Use of the no-slip conditions at the interfaces,

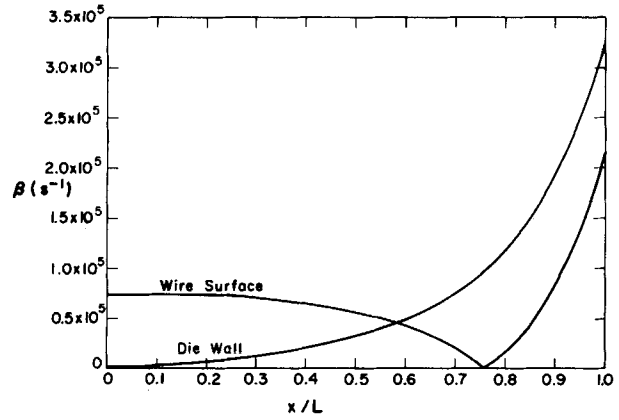

Figure 8. Approximate surface shear rates for a wire-coating operation.

$$V_x = V_w \text{ at } r = R_1 \tag{81}$$

$$V_x = 0 \text{ at } r = a(x)R_1 \tag{82}$$

and the given mass flow rate,

$$w = 2\pi\rho \int_{R_1}^{aR_1} V_x r dr \tag{83}$$

leads to three equations for the three functions $f_i(x)$:

$$f_0(x) + f_2(x) = 1 \tag{84}$$

$$f_0(x) + f_1(x)\, ln\, a(x) + f_2(x)a^2(x) = 0 \tag{85}$$

$$a^2(L) - 1 = \int_1^{a(x)} 2[f_0(x) + f_1(x)\, ln\, u + f_2(x)u^2]u du. \tag{86}$$

Here w has been chosen so that there is no draw-down, i.e., the final coating diameter matches the exit diameter of the die.

From Eq. 80 the shear rates at the die wall and wire surface are

$$\beta_d = \left|\frac{V_w}{R_1}\left[\frac{f_1(x)}{a(x)} + 2a(x)f_2(x)\right]\right| \tag{87}$$

$$\beta_w = \left|\frac{V_w}{R_1}[f_1(x) + 2f_2(x)]\right| \tag{88}$$

These functions are plotted in Figure 8. The shear rate at the die wall rises monotonically to a maximum of $3.2 \times 10^5\ s^{-1}$, while the shear rate at the wire first declines to zero and then rises to $2.1 \times 10^5\ s^{-1}$ as the neighboring fluid elements accelerate from velocities below to above that of the wire.

Carley, Endo, and Krantz (1978) have provided property data for a representative low-density polyethylene melt. For the boundary regions, their shear stress model reduces to

$$\tau_{rz} = -m_T\left|\frac{\partial V_z}{\partial r}\right|^{-2/3}\frac{\partial V_z}{\partial r} \tag{89}$$

with

$$m_T = m_0 \exp\left[\frac{E}{3R}\left(\frac{1}{T} - \frac{1}{T_{ref}}\right)\right] \tag{90}$$

and

$$m_0 = 1.01 \times 10^4\ kg \cdot m^{-1} \cdot s^{-5/3}$$
$$E/R = 5.89 \times 10^3\ K$$
$$T_{ref} = 479\ K.$$

The factor $\frac{1}{3}$ in Eq. 90 is the ratio of the activation energies at constant $\partial V_z/\partial r$ and at constant τ_{rz}, calculated for this model by the "method of reduced variables" (Bird, Armstrong and Hassager, (1977). In this analysis m_T is evaluated at an average temperature as described below. The following properties are also treated as independent of temperature:

$$k = 0.329\ W \cdot m^{-1} \cdot K^{-1}\ (7.86 \times 10^{-4}\ cal \cdot s^{-1} \cdot cm^{-1} \cdot K^{-1})$$

$$\rho\hat{C}_p = 2.1 \times 10^6\ J \cdot m^{-3} \cdot K^{-1}\ (0.50\ cal \cdot cm^{-3} \cdot K^{-1})$$

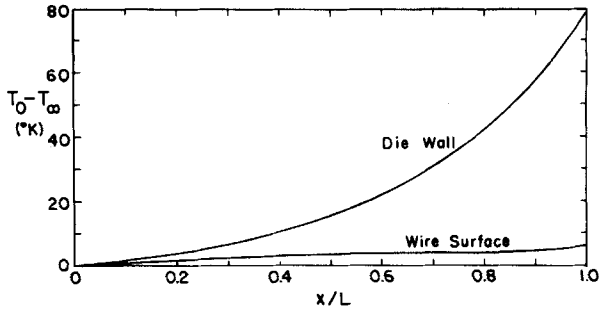

Figure 9. Surface temperature rises for an adiabatic wire-coating operation.

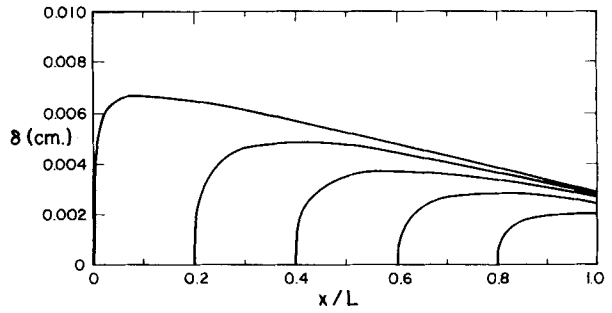

Figure 10. Thermal boundary layer development in a wire-coating system.

The surfaces of the wire-coating system are assumed adiabatic. At the die wall we use $h_x \doteq 1$ and $h_z = a(x)R_1$. Equations 46, 87 and 89 then give the die wall temperature distribution

$$T_{0,A}^{(t)} - T_\infty = \frac{9^{2/3}\, g(0)}{\rho\hat{C}_p\alpha^{1/3}} m_T \times \left[\left(\int_{x_1=0}^{x}\sqrt{a\beta_d}\, a dx_1\right)^{2/3}\left|\frac{\beta_d^{1/3}}{a}\right|_{\xi=0} + \int_{\xi=0}^{x}\left(\int_{x_1=\xi}^{x}\sqrt{a\beta_d}\, a\, dx_1\right)^{2/3} d\left[\frac{\beta_d^{1/3}(\xi)}{a(\xi)}\right]\right] \cdot \tag{91}$$

for adiabatic operation. The first term of Eq. 91 accounts for the assumed initial jump in wall shear rate, and the second term accounts for all subsequent changes. Integration by parts, or use of Eq. 47, gives a simpler result:

$$T_{0,A}^{(t)} - T_\infty = \frac{9^{2/3}\, g(0)}{\rho\hat{C}_p\alpha^{1/3}} m_T \int_{\xi=0+}^{x}\frac{2}{3} \times \left(\int_{x_1=\xi}^{x}\sqrt{a\beta_d}\, a\, dx_1\right)^{-1/3}(\beta_d^{1/3}\sqrt{a\beta_d})|_\xi d\xi. \tag{92}$$

The index m_T is evaluated from Eq. 90 at the mean of the entrance and exit surface temperatures; this entails an iterative calculation.

The temperature rise at the moving wire surface is obtained from Eqs. 55, 88 and 89, with $t = x/V_w$ and $-(\boldsymbol{\tau}:\nabla \boldsymbol{V}) = \tau_0\beta_w$. The result is

$$T_0^{(o)} - T_\infty = \frac{m_T}{\rho\hat{C}_p V_w}\int_{x_1=0}^{x}\beta_w^{4/3}\, dx_1. \tag{93}$$

The index m_T is again evaluated at the mean of the entrance and exit surface temperatures. Equation 15 is equivalent to Eq. 55 here since the system is at steady state when viewed from the die.

Numerical integration of Eqs. 91 and 93 with $T_\infty = T_{ref}$ gives the results shown in Figure 9. The temperature at the die wall rises from 479 to 558 K; this increase is comparable to the results obtained numerically by Carley, Endo and Krantz (1978) for similar wire-coating systems. The calculated temperature rise at the wire surface is much smaller (only 6.1 K at the maximum) and would be still less if we had included heat transfer to the moving wire.

The boundary layer thickness associated with each increment of τ_0/h_z along the die wall is obtainable from Eqs. 32 and 87:

$$\delta(x,\xi) = \frac{1}{\sqrt{a\beta_d}}\left\{9\alpha \int_{x_1=\xi}^{x} \sqrt{a\beta_d}\, a\, dx_1\right\}^{1/3} \tag{94}$$

Figure 10 shows the growth of five representative boundary layers emanating from equally spaced points along the die wall. Each of these layers grows rapidly at first, but then gets thinner as the flow converges and accelerates. The final thickness of the layer associated with the initial jump in τ_0 is 0.0029 cm (0.0011 in.), or 11% of the final coating thickness. The boundary layer on the wire is still thinner because of the short residence time. Thus, the small-diffusivity assumption of the analysis is accurate here.

ACKNOWLEDGMENT

This work was supported by the National Science Foundation through Grant CPE79-13162, and by the U.S. Army under Contract DAAG29-80-C-0041.

NOTATION

a = length of side of equilateral triangle (L); radius ratio in Eqs. 78–79
$B(m,n)$ = $\Gamma(m)\Gamma(n)/\Gamma(m+n)$
$\hat{C}_p$ = heat capacity at constant pressure ($EM^{-1}T^{-1}$)
$\frac{D}{Dt}$ = $\left.\frac{\partial}{\partial t}\right|_r + (V\cdot\nabla)$, substantial derivative (t^{-1})
(E) = unit of energy (ML^2t^{-2})
E = activation energy in Eq. 90 (E mol^{-1})
F = dimensionless function defined in Eq. 67
f = friction factor, Eq. 72
f = function defined in Eq. 23 (T)
$f''(0,m)$ = dimensionless shear stress at wedge surface, Eq. 57
f_0,f_1,f_2 = dimensionless functions defined in Eq. 80
G = dimensionless function defined in Eq. 68
g = dimensionless temperature function defined in Eq. 23
h_x,h_y,h_z = scale factors defined in Eq. 3
k = thermal conductivity ($Et^{-1}L^{-1}T^{-1}$)
(L) = unit of length
L = length of channel (L)
l = arc length along a streamline (L)
(M) = unit of mass
m = dimensionless parameter defined in Eq. 59
m_T = material function in power law model, Eq. 89
$O(y^n)$ = terms of order n or greater in y
P = $p + \rho\hat{\Phi}$ $ML^{-1}t^{-2}$)
$P_0 - P_L$ = decrease of P along duct length $L(ML^{-1}t^{-2})$
Pr = Prandtl number
p = pressure ($ML^{-1}t^{-2}$)
q_0 = conductive heat flux into the stream at $y = 0$ ($EL^{-2}t^{-1}$)
R = gas constant in Eq. 90 (E mol$^{-1}T^{-1}$)
R = radius of sphere or cylinder (L)
Re = Reynolds number
R_1 = wire radius (L)
$R_2(x)$ = local radius of wire-coating die (L)
r = position vector (L)
r = radial coordinate (L)
r = dimensionless ratio C_1/C_0, Eq. 34
T = absolute temperature (T)
t = time (t)
U = local free stream velocity for wedge flow (Lt^{-1})
$\langle V\rangle$ = mean velocity through cross section of pipe (Lt^{-1})
V = velocity vector relative to nondeforming coordinates (Lt^{-1})
V = magnitude of velocity vector (Lt^{-1})
V_w = velocity of wire or moving wall (Lt^{-1})
V_x,V_y,V_z = components of velocity vector (Lt^{-1})
V_r,V_θ = velocity components in cylindrical or spherical coordinates (Lt^{-1})
V_t = magnitude of tangential velocity vector (Lt^{-1})
V_∞ = magnitude of free stream velocity (Lt^{-1})
X_1,X_2,X_3 = material coordinates (arbitrary units)
x = surface coordinate directed along surface streamlines; Eqs. 3–6 (Lh_x^{-1})
Y = half width of slit (L)
y = normal distance from interface (L)
Z = cylindrical axial coordinate (L)
z = surface coordinate normal to the local x-direction; Eqs. 3–6 (Lh_z^{-1})

Greek Letters

α = $k/\rho\hat{C}_p$, thermal diffusivity (L^2t^{-1})
β = $(\partial V_t/\partial y)|_{y=0}$, function introduced in Eq. 4 (t^{-1})
$\Gamma(x)$ = $\int_0^\infty e^{-z}z^{x-1}dz$
γ = Euler's constant, 0.57721 . . .
δ = boundary layer thickness for viscous heating or heat transfer (L)
$\boldsymbol{\delta}_x,\boldsymbol{\delta}_y,\boldsymbol{\delta}_z$ = unit vectors
ϵ = special dissipation function for fundamental solution, Eqs. 19 and 43 ($EL^{-3}t^{-1}$)
η = dimensionless coordinate defined in Eq. 24
θ = angle in cylindrical or spherical coordinates (radians)
θ = wedge angle (radians)
κ = ratio of inner cylinder radius to outer
μ = viscosity ($ML^{-1}t^{-1}$)
ν = μ/ρ kinematic viscosity (L^2t^{-1})
ξ = value of x at the jump in ϵ and $T^{*(i)}$
Π = dimensionless temperature function in Eq. 49
ρ = density (ML^{-3})
σ = $(x/R)(R\langle V\rangle/\nu)^{-1}$, dimensionless downstream coordinate in tube
τ = stress tensor ($ML^{-1}t^{-2}$)
τ_0 = magnitude of tangential stress at interface ($ML^{-1}t^{-2}$)
$\hat{\Phi}$ = gravitational potential energy (L^2t^{-2})
ϕ = angle in spherical coordinates (radians)
ω = angular velocity of rotating disk (radians t^{-1})
ψ_1,ψ_2 = stream functions, Eq. 7

Superscripts

(i) = inner solution
(o) = outer solution
$*$ = solution with special dissipation function $\epsilon(x,\xi,z)$.

Subscripts

A = dissipative solution for adiabatic boundary
d = at die wall
w = at wire surface
0 = in or into the fluid at $y = 0$; upstream value of P
∞ = upstream or initial temperature
1 = dummy variable or first stream function

LITERATURE CITED

Bird, R. B., W. E. Stewart, and E. N. Lightfoot, *Transport Phenomena*, Wiley, New York (1960).

Bird, R. B., R. C. Armstrong, and O. Hassager, *Dynamics of Polymeric Liquids: Vol. I Fluid Mechanics*, Wiley, New York, p. 189, 306 (1977).

Carley, J. F., T. Endo, and W. B. Krantz, "Realistic Analysis of Flow in Wire-Coating Dies," *Soc. of Plastic Eng.*, **36**, 453 (1978).

Cochran, W. G., "The Flow Due to a Rotating Disc," *Proc. Cambr. Phil. Soc.*, **30**, 365 (1934).
Haas, K. U., and F. H. Skewis, "The Wire-Coating Process; Die Design and Polymer Flow Characteristics," *Soc. of Plastic Eng.*, **32**, 8 (1974).
Hartree, D. R., "On an Equation Occurring in Falkner and Skan's Approximate Treatment of the Equations of the Boundary Layer," *Proc. Cambr. Phil. Soc.*, **33**, 223 (1937).
Hornbeck, R. W., "Laminar Flow in the Entrance Region of a Pipe," *App. Sci. Res.*, **13**, 224 (1964).
Landau, L., and E. M. Lifshitz, *Fluid Mechanics*, Addison-Wesley, Reading, MA (1960).
Lighthill, M. J., "Contributions to the Theory of Heat Transfer Through a Laminar Boundary Layer," *Proc. Roy. Soc.*, **A202**, 359 (1950).
Meksyn, D., "Plate Thermometer," *ZAMP*, **11**, 63 (1960).
Pohlhausen, E., "Der Wärmeaustauch zwischen festen Körpern und Flüssigkeiten mit kleiner Reibung und kleiner Wärmeleitung," *ZAMM*, **1**, 115 (1921).
Rosenhead, L., *Laminar Boundary Layers*, Oxford University Press, Oxford (1963).
Schlichting, H., *Boundary Layer Theory*, 4 Ed., McGraw-Hill, New York (1960).
Stewart, W. E., "Forced Convection in Three-Dimensional Flows: I. Asymptotic Solutions for Fixed Interfaces," *AIChE J.*, **9**, 528 (1963).
Stewart, W. E., J. B. Angelo, and E. N. Lightfoot, "Forced Convection in Three-Dimensional Flows: II. Asymptotic Solutions for Mobile Interfaces," *AIChE J.*, **16**, 771 (1970).

Manuscript received November 4, 1981; revision received October 15 and accepted October 28, 1982.

Separating Efficiency of a Water Elutriator

This paper investigates the separating efficiency of a vertical water elutriator operating on particle mixtures. In particular, comparisons are made with a previously developed mathematical model based on an eddy diffusion mechanism of mixing. Standard mixtures of glass spheres, of uniform size and shape, are used to study the equipment characteristics. It is found that the separating efficiency follows the same trend as predicted by the model and that "wall flow" of particles occurs. This affects the required water velocity, resulting in the equipment producing a top product generally purer than the bottom product.

M. W. BIDDULPH

Department of Chemical Engineering
University of Nottingham
Nottingham, England

SCOPE

The field of waste recycling and the recovery of useful materials from waste will continue to become more important as the supplies of natural resources decrease. Unfortunately, unless some form of source segregation has occurred, the feedstock which presents itself for separation is usually in the form of a complicated mixture of solid particles emerging from a grinder. One of the key separating stages is often water elutriation or air classification, methods which rely on differences in terminal falling velocities between different particles. Although these have often been set up in various forms, little work has been directed towards obtaining a better understanding of their operation, and hence improving their efficiency. A new aspect of the problem in the application to waste streams is that the size and density of the solid particles is such that higher fluid velocities are required than in application to very fine particle mixtures. This introduces fluid turbulence which affects the behavior of the equipment.

The study described in this paper is part of a continuing effort to improve the separating efficiency of this type of equipment. Early work on a small water elutriator is now extended to a much larger-scale model. Standard mixtures of uniform particles are separated. Glass spheres were chosen as requiring similar water velocities to those often encountered in waste recycling operations. A previously developed mathematical model, using an eddy diffusion mechanism superimposed on the expected convective movement of particles, is compared with the actual separation obtained from the equipment.

CONCLUSIONS AND SIGNIFICANCE

The study has demonstrated the presence and significance of the "wall flow" of particles in a vertical water elutriator. This refers to the tendency of particles to cluster together and migrate to the slower moving fluid near the tube wall, rather than remaining near the axis of the tube. This results in the required average fluid velocity being about 5–15% greater than would be expected; the "light" species, trying to move upwards to the top product, can penetrate very significantly downwards to appear in the bottom product. The fluid turbulence means that the "heavy" species can also penetrate upwards towards the top product, and it has been found that this can be predicted satisfactorily using values of eddy diffusivity obtained by Levenspiel for single-phase dispersion coefficients in pipe flow. However, the wall-flow effect means that values of diffusivity of about 2.5 times the Levenspiel value are required for the "light" species penetrating downwards. The optimum separation can be predicted well using this model.

We may conclude that the simple vertical water elutriator is better at producing a pure top product than at producing a pure bottom product; therefore, the point of solids injection should be nearer the top than the bottom. The results give some encouragement that the model will help to clarify the characteristics of this type of equipment, and it is hoped to extend the study to mixtures containing ranges of shapes, densities and sizes, and to relate separating efficiency to the method of grinding the feedstock. Methods of avoiding wall flow are to be studied as well as the application to air classifiers.